Hybrid Hartree-Fock density functional study of charged point defects in ferroelectric PbTiO₃

Takahiro Shimada,[1,*] Taku Ueda,[1] Jie Wang,[1,2] and Takayuki Kitamura[1]

[1]*Department of Mechanical Engineering and Science, Kyoto University, Nishikyo-ku, Kyoto 615-8540, Japan*
[2]*Department of Engineering Mechanics, School of Aeronautics and Astronautics, Zhejiang University, Hangzhou 310027, China*

The nature of intrinsic point defects, i.e., energetic, ferroelectric, and electronic properties of vacancies in ferroelectric PbTiO₃, is studied using first-principles calculations based on the hybrid Hartree-Fock density functional, which correctly reproduces the band gap and thus provides the accurate defect electronic states. The oxygen vacancies are found to behave as double shallow donors and are thermodynamically stable over a wide range of Fermi levels under oxygen-poor conditions, while Pb vacancies are likely to be formed under oxygen-rich conditions and act as double shallow acceptors, which lead to p-type conductivity. The result shows good consistency with the relevant experimental observations. The ferroelectric distortion is disturbed anisotropically outward by oxygen vacancies and is characterized by localized defect electronic states contributed by d orbitals. In contrast, an isotropically inward ferroelectric disturbance is found around Pb and Ti vacancies. Such a ferroelectric disturbance is strongly enhanced by the charging of vacancies, except for Pb vacancies that induce delocalized defect states.

　　　　　PACS number(s): 77.80.−e, 61.72.jd, 31.15.A−

I. INTRODUCTION

Ferroelectric perovskite oxides, such as PbTiO₃ and the Pb(Zr,Ti)O₃ solid solution, are electroceramic materials that exhibit ferroelectricity and related electromechanical properties, including a large piezoelectric response and a high dielectric constant.[1] The outstanding versatility of their multiple functionalities has drawn significant attention to the ferroelectric perovskite oxides for technological applications, such as high-density nonvolatile random access memories (FeRAMs), transducers, sensors, and electromechanical devices.[2,3]

Ferroelectric perovskite oxides usually contain many defects that are included during the growth or production processes.[4–7] Vacancies, which are among the important point defects in solids, are reported to have a significant influence on the ferroelectricity and related properties of solids, as confirmed by both experimental and theoretical studies:[8–14] Ferroelectricity generally originates from the delicate balance between short-range covalent and/or repulsive interactions and long-range Coulombic interactions.[15–18] The appearance of vacancies causes a partial loss of short-range interactions. The balance of long-range Coulombic interactions is also broken by positively or negatively charged vacancies. Thus, ferroelectricity can be strongly affected by vacancies. In addition, vacancies play a significant role in polarization fatigue, imprinting, and degradation during poling and reversal processes, in addition to piezoelectric response through the pinning of spontaneous polarization or domain walls.[8–14] Specific vacancies are also considered to be a source of electric current leakage,[4,5,19,20] which often leads to a critical malfunction in ferroelectric and electromechanical devices. These characteristics of point defects in ferroelectric materials are closely associated with and predominated by distinctive electronic structures induced by vacancies: the so-called defect state. It is therefore essential to achieve a fundamental understanding of the defect-state characteristics of vacancies in ferroelectrics from both atomistic and electronic perspectives.

First-principles density functional theory (DFT)[21,22] calculations have been commonly used to study the electronic properties of point defects in insulators and semiconductors. The local density approximation (LDA)[23] or the generalized gradient approximation (GGA)[24,25] functionals are typically employed to describe the exchange-correlation energy within DFT. However, it is well known that the LDA and GGA tend to underestimate the band gaps of insulators and semiconductors, which causes a serious problem in describing the electronic structure of point defects: The defect state is often introduced between the valence band maximum (VBM) and conduction band minimum (CBM), i.e., in the band gap. With the LDA or GGA functionals, the defect level is, however, embedded in conduction bands due to underestimation of the band gap, which leads to a critical misprediction of the electronic structures of point defects in insulators.[26–29] For the case of ferroelectric PbTiO₃, the band gap is evaluated as 1.62 eV using the LDA functional,[30] which has been commonly used to investigate the vacancies of PbTiO₃ in previous works,[11,31–39] but is less than half of the experimental value of 3.4 eV.[40] Thus, the previous results using the LDA functional suffer from a serious underestimation of the band gap. It is therefore necessary to accurately reproduce the band gap for investigations of the electronic and atomic structures of vacancies in ferroelectric PbTiO₃.

Heyd *et al.* recently proposed hybrid Hartree-Fock (HF) density functionals,[41] which include in part the exact nonlocal exchange of HF theory to DFT. The hybrid functional has been used to accurately reproduce the band gaps of insulators and semiconductors[42]; therefore, the use of the hybrid functional is rationalized for the description of defect physics. This validation has resulted in application to point defects in various oxide materials[26–29]; however, there have been no reports that have addressed vacancies in ferroelectric PbTiO₃ using the hybrid functional.

TABLE I. Calculated lattice parameters, a and c, tetragonality c/a, and band gap E_{gap} of ferroelectric $PbTiO_3$ using LDA, GGA-PBE, GGA-PBEsol, LDA + U, PBE + U, PBEsol + U, and the HSE06 hybrid functional. The optimal on-site Coulomb and exchange parameters for Ti-d orbitals, $U = 5.0$ eV and $J = 0.64$ eV, respectively, are used for all the DFT + U calculations. The experimental values[40,47] are also listed for comparison. The error from the experimental values is shown in parentheses.

	LDA	GGA-PBE	GGA-PBEsol	LDA + U	PBE + U	PBEsol + U	HSE06	Expt.
a (Å)	3.867	3.841	3.876	3.918	3.985	3.935	3.855	3.88
	(−0.3%)	(−1.0%)	(−0.1%)	(+1.0%)	(+2.7%)	(+1.4%)	(−0.7%)	
c (Å)	4.042	4.736	4.150	3.951	4.091	3.979	4.120	4.155
	(−2.7%)	(+14.0%)	(−0.1%)	(−4.9%)	(−1.5%)	(−4.2%)	(−0.8%)	
c/a	1.045	1.233	1.071	1.008	1.026	1.011	1.071	1.071
E_{gap} (eV)	1.62	2.04	2.08	2.41	2.50	2.49	3.41	3.4
	(−52%)	(−41%)	(−40%)	(−30%)	(−28%)	(−28%)	(+0.3%)	

In this paper, we perform first-principles calculations based on the hybrid HF density functional in conjunction with appropriate treatment of a periodic finite-size supercell to provide accurate energetic, ferroelectric, and electronic properties for native point defects in ferroelectric $PbTiO_3$. This paper is organized as follows. Section II describes the detailed simulation models and procedure, in addition to the validity and effectiveness of the hybrid functional for application to $PbTiO_3$. Section III A describes the thermodynamic stability, charge states, and transition levels of vacancies. The ferroelectric properties that result from vacancies are presented in Sec. III B, the magnetic properties induce by vacancies are shown in Sec. III C, and the defect electronic states and levels are analyzed in Sec. III D. Finally, Sec. IV summarizes the results.

II. COMPUTATIONAL DETAILS

A. Simulation method

Ab initio (first-principles) calculations based on (generalized) Kohn-Sham theory[22] were performed using the Vienna *Ab initio* Simulation Package (VASP) code.[43,44] The electronic wave functions are expanded as plane waves up to a cut-off energy of 500 eV. The electron-ion interaction is represented by the projector-augmented wave method.[45,46] The Pb $5d$, $6s$, and $6p$, the Ti $3s$, $3p$, $3d$, and $4s$, and the O $2s$ and $2p$ electrons are explicitly treated as valence states. Spin polarization is considered for all calculations. The exchange-correlation energies are described by the Heyd-Scuseria-Ernzerhof (HSE06) screened hybrid functional,[41] which includes in part the exact nonlocal exchange of HF theory into the Perdew-Burke-Ernzerhof functional (PBE)[25] of the GGA. The exchange potential is evaluated by mixing 25% of the HF exchange with 75% of the PBE exchange as Heyd *et al.* suggested,[41] while electronic correlation is essentially represented by the PBE functional. A screening parameter of 0.2 Å^{-1} is used for the semilocal PBE exchange and the screened nonlocal exchange.

The validity and effectiveness of the HSE06 hybrid functional is carefully tested for $PbTiO_3$ by comparing available exchange-correlation functionals. Table I lists the structural parameters and band gap of ferroelectric $PbTiO_3$ obtained experimentally and by using various functionals, where a and c are the lattice parameters of tetragonal $PbTiO_3$. LDA

and GGA-PBEsol, which is a GGA-PBE functional revised for solids and surfaces,[48] provide good structural predictions; however, the band gap is underestimated by 40–50%. Although a slight improvement can be found using the DFT + U method[49] with the optimal on-site Coulombic and exchange parameters for Ti-d orbitals, $U = 5.0$ eV and $J = 0.64$ eV, respectively,[50] a 30% error in the band gap still exists, and the structural prediction becomes worse. In contrast, the HSE06 hybrid functional successfully reproduces both the lattice parameters and the band gap with extremely high accuracy (errors less than 1%). This result clearly indicates that the HSE06 hybrid functional is capable of accurately describing the electronic and structural properties of point defects in ferroelectric $PbTiO_3$.

B. Simulation models and procedure

Figure 1 shows the simulation model for a vacancy in ferroelectric $PbTiO_3$ with a polar axis of [001]. We employ a $3 \times 3 \times 3$ simulation supercell containing 135 atoms, in
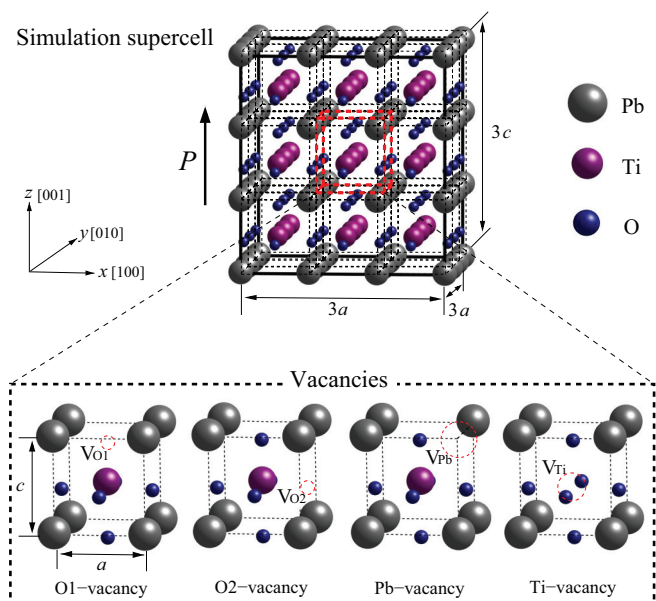
FIG. 1. (Color online) Simulation models for O1, O2, Pb, and Ti vacancies in ferroelectric $PbTiO_3$. The P arrow indicates the spontaneous polarization.

which three perovskite unit cells are arranged along the x, y, and z direction. The simulation cell dimensions are $L_x = 3a$, $L_y = 3a$, and $L_z = 3c$. A vacancy, denoted as V_α^q ($\alpha = $ O1, O2, Pb, and Ti), is introduced by removing one corresponding atom from the simulation supercell. Here, the oxygens, O1 and O2, which are located in the polar [001] direction and the nonpolar [100] or [010] direction relative to the Ti atom, respectively, are not equivalent to each other due to the tetragonal symmetry (space group $P4mm$). q denotes the charge state of the vacancy, and all possible charge states ($q = 0 \sim 2+$ for the O1 and O2 vacancies, $q = 0 \sim 2-$ for the Pb vacancy, and $q = 0 \sim 4-$ for the Ti vacancy) are considered in this study.

$2 \times 2 \times 2$ Monkhorst-Pack k-point sampling[51] is used for the Brillouin zone integrations. The atomic configuration is fully relaxed using the conjugate gradient method until the Hellmann–Feynman forces are less than 0.01 eV/Å. To provide correct energies for the supercells containing a charged defect, a homogeneous background charge is added and undesirable monopole-monopole (first-order) interactions are explicitly corrected.[34,52,53] The remaining higher order uncertainties with respect to the size of supercell are also implicitly corrected using the finite-size scaling procedure.[34,52,54] Note that the different sizes of the simulation supercell, from $2 \times 2 \times 2$ to $3 \times 3 \times 3$, are also simulated in the same manner to perform the finite-size scaling correction.

III. RESULTS AND DISCUSSIONS

A. Stability of vacancies and charged states

1. Vacancy formation energy and chemical stability range

To investigate the stability of vacancies in PbTiO$_3$ and their charged states, we introduce the vacancy formation energy

$$E_{\text{vf}}\left(V_\alpha^q\right) = \left[E_{\text{tot}}\left(V_\alpha^q\right) + \mu_\alpha + q(E_{\text{VBM}} + \varepsilon_{\text{F}})\right] - E_{\text{tot}}(\text{perfect}),$$
$$(1)$$

where $E_{\text{tot}}(V_\alpha^q)$ is the total energy of a supercell with a vacancy V_α^q, and $E_{\text{tot}}(\text{perfect})$ is the total energy of a supercell for perfect (defect-free) PbTiO$_3$. E_{VBM} and ε_{F} are the VBM of PbTiO$_3$ with a potential alignment correction[37,55] and the Fermi level measured from the VBM, respectively. ε_{F} can vary from the VBM to the CBM. μ_α denotes the chemical potential of atom α in PbTiO$_3$, the valid range of which is discussed below.

The chemical potential generally varies with the surrounding environment. A valid range for the chemical potential of PbTiO$_3$ can be determined from the thermodynamic equilibrium conditions and the requirement to prevent the formation of other solid solutions or secondary phases.

(i) The chemical potential of the α atom in PbTiO$_3$ μ_α should be lower than that of an elemental solid consisting of only α atoms μ_α^{elem}, to ensure the elemental solid does not precipitate. Note that μ_O^{elem} is given by half of the total energy of an O$_2$ molecule under the consideration of spin-polarization. This requirement is given by

$$\Delta\mu_{\text{Pb}} \leqslant 0, \quad \Delta\mu_{\text{Ti}} \leqslant 0, \quad \Delta\mu_{\text{O}} \leqslant 0, \quad (2)$$

where $\Delta\mu_\alpha = \mu_\alpha - \mu_\alpha^{\text{elem}}$ is the difference in the chemical potentials of the α atom in PbTiO$_3$ and the corresponding elemental solid.

TABLE II. Formation enthalpies (in eV) of PbO, TiO$_2$, and PbTiO$_3$ calculated from the HSE06 hybrid functional. The result obtained from the GGA-PBE functional and experimental values[56] are also listed for comparison.

	HSE06	GGA-PBE	Experiment
ΔH(PbO)	−2.277	−2.25	−2.27
ΔH(TiO$_2$)	−10.017	−9.13	−9.79
ΔH(PbTiO$_3$)	−12.560	11.64	–

(ii) According to the thermodynamic equilibrium condition, the sum of the chemical potentials of atoms in PbTiO$_3$ must be equal to the heat of formation to ensure the stability of the compound PbTiO$_3$. This condition can be formulated as

$$\Delta H(\text{PbTiO}_3) \equiv (\mu_{\text{Pb}} + \mu_{\text{Ti}} + 3\mu_{\text{O}})$$
$$- \left(\mu_{\text{Pb}}^{\text{elem}} + \mu_{\text{Ti}}^{\text{elem}} + 3\mu_{\text{O}}^{\text{elem}}\right)$$
$$= \Delta\mu_{\text{Pb}} + \Delta\mu_{\text{Ti}} + 3\Delta\mu_{\text{O}}, \quad (3)$$

where $\Delta H(\text{PbTiO}_3)$ denotes the formation enthalpy of PbTiO$_3$.

(iii) The chemical potentials should be lower than the formation enthalpy of other possible compounds of PbO and TiO$_2$ to avoid the formation of binary compounds:

$$\Delta\mu_{\text{Pb}} + \Delta\mu_{\text{O}} \leqslant \Delta H(\text{PbO}), \quad (4)$$

$$\Delta\mu_{\text{Ti}} + 2\Delta\mu_{\text{O}} \leqslant \Delta H(\text{TiO}_2). \quad (5)$$

The formation energy should be evaluated within the valid range of chemical potentials that satisfy Eqs. (2)–(5).

The formation enthalpies of the PbO, TiO$_2$, and PbTiO$_3$ compounds obtained using the present HSE06 hybrid functional are listed in Table II. The experimental values[56] and those obtained previously using the GGA-PBE functional[39] are also shown for comparison. The formation enthalpies obtained with the present HSE06 functional calculations are in excellent agreement with the experimental values and are better than those obtained with the GGA-PBE functional. This agreement clearly demonstrates the reliability of the present calculations. Figure 2 shows the phase diagram for PbO, TiO$_2$, and PbTiO$_3$. The red area indicates the chemically stable region of PbTiO$_3$ obtained from Eqs. (2)–(5). Here, the chemical potential $\Delta\mu_\alpha$, generally reflects the environmental conditions. For example, at the top-right points of A and B, at the boundary of chemical stability range of PbTiO$_3$, $\Delta\mu_{\text{O}}$ has relatively small values of -2.27 and -2.54 eV, respectively, which correspond to oxygen-poor conditions. In contrast, $\Delta\mu_{\text{O}}$ is zero at the bottom-left border points of C and D, which correspond to oxygen-rich conditions. The oxygen-poor (point A) and oxygen-rich (point D) conditions are the primary focus in the following discussion.

2. Stability of vacancies

Figure 3 plots the vacancy formation energy E_{vf}, as a function of ε_{F} for each vacancy under the oxygen-poor condition (point A). Here we present the formation energies after the corrections described in Sec. II; therefore, the energies are free from any undesirable interactions and uncertainties from the finite size of the supercell. Note that the magnitude of
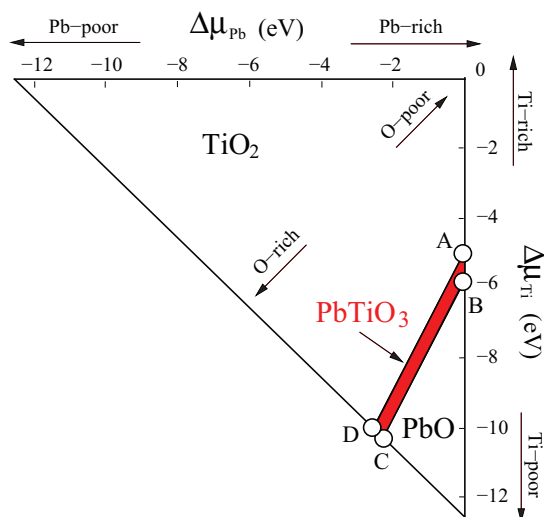
FIG. 2. (Color online) Phase diagram of tetragonal PbTiO$_3$. The red-colored area shows the chemical stability range of PbTiO$_3$. Points A and B correspond to oxygen-poor (O-poor) limit, while points C and D correspond to oxygen-rich (O-rich) limit.

corrections for the defect-formation energies are 0.08–0.34 eV, 0.2–0.4 eV, and 0.01–0.05 eV for the monopole-monopole correction for charged cell,[34,52,53] the finite-size scaling with respect to the finite supercell size,[34,52,54] and the band-alignment correction,[37,55] respectively. Thus, the corrections related to the finite size of supercells must be critical for the evaluation of defect-formation energies, while the band-alignment correction affects the result less. For the O1 vacancy, the vacancy-formation energy of the neutral V_{O1}^0, is a high and positive value of 2.94 eV, while the charged O1 vacancies have lower and negative formation energies (−0.40 eV for V_{O1}^+ and −3.76 eV for V_{O1}^{2+}) at the VBM. This indicates that the charged O1 vacancies can form spontaneously during PbTiO$_3$ crystal growth when the Fermi level is near the VBM, whereas it is difficult for the neutral O1 vacancy to form, even under oxygen-poor conditions. A comparison of the charge states indicates that the formation energy of V_{O1}^{2+} is approximately 3 eV lower than V_{O1}^+ at the VBM. The O1 vacancy is thus preferentially doubly ionized, so that the other charge states are unlikely to appear near the VBM. The situation changes when the Fermi level is increased from the VBM to the CBM. The formation energy of the charged O1 vacancies increases with the increase of the Fermi level. When the Fermi level is near the CBM, the O1 vacancies
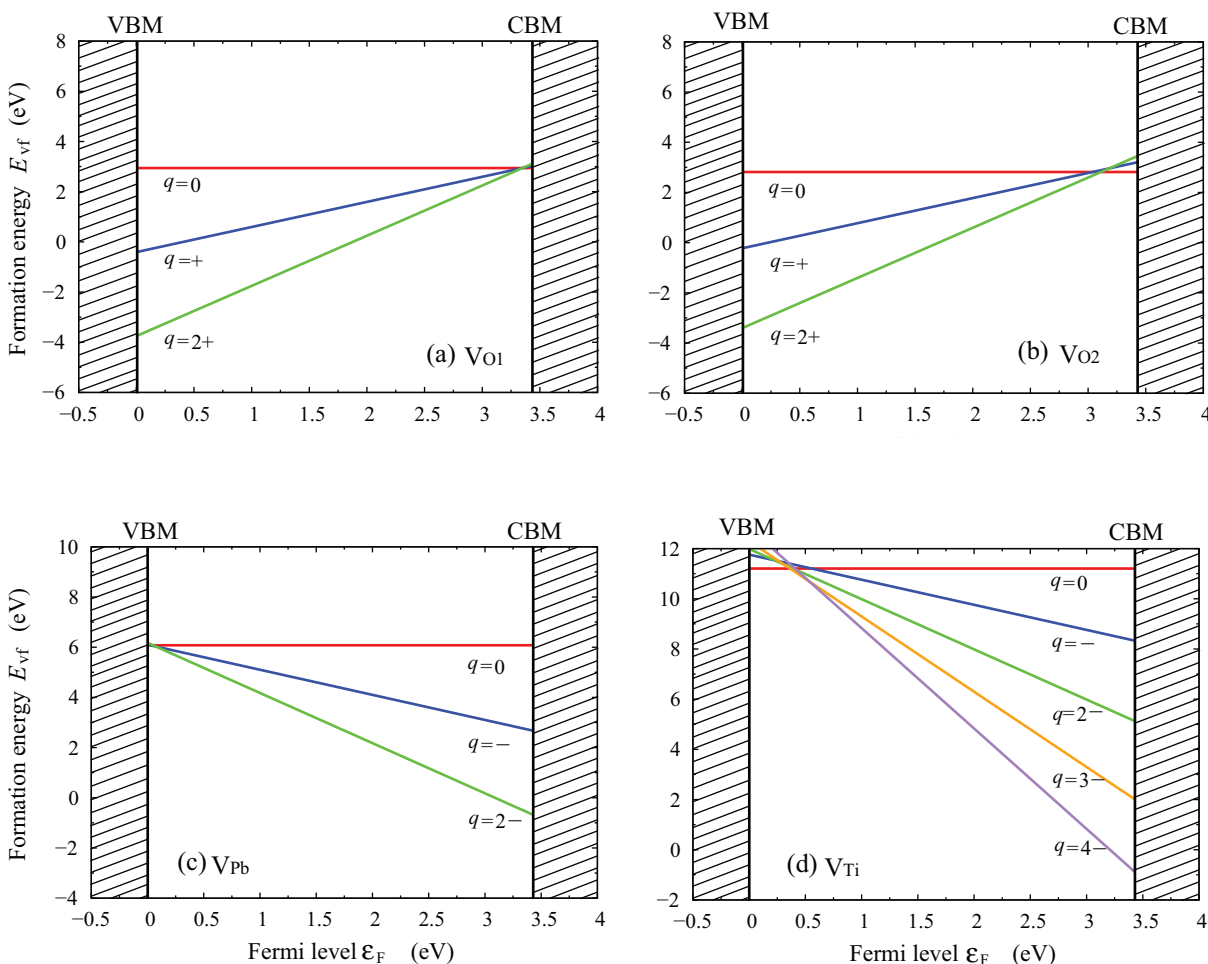
FIG. 3. (Color online) Vacancy formation energies E_{vf} of (a) V_{O1}, (b) V_{O2}, (c) V_{Pb}, and (d) V_{Ti} as a function of Fermi level ε_F under the O-poor limit (point A). The q indicates the charge state of each vacancy.
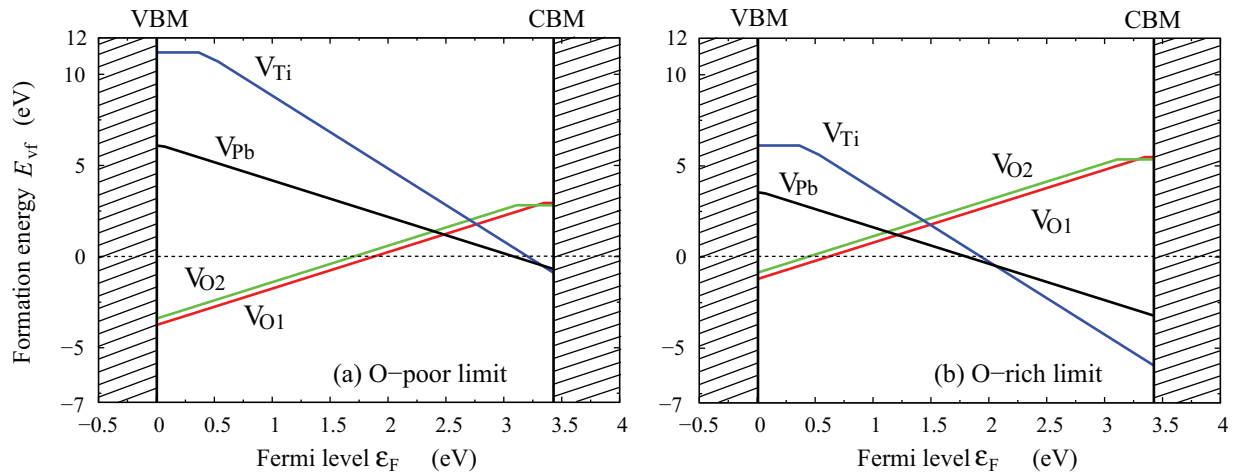
FIG. 4. (Color online) Vacancy formation energies E_{vf} of V_{O1}, V_{O2}, V_{Pb}, and V_{Ti} as a function of Fermi level ε_F under the (a) O-poor limit (point A) and (b) O-rich limit (point D).

with three different charge states have a large and positive formation energy of approximately 2.9 eV. This suggests that the O1 vacancy is unlikely to form near the CBM. Note that the lowest energy charge state changes from 2+ to neutral when the Fermi level reaches $\varepsilon_F = 3.3$ eV, which suggests a 2+/0 charge transition level of the O1 vacancy. The transition level will be discussed in the next section.

The O2 vacancies exhibit similar energetics to the O1 vacancies, except that the formation energies of the O2 vacancies are slightly higher (ca. 0.1 eV) than those of the O1 vacancies [see Fig. 3(b)]. The difference between the O1 and O2 vacancies results from their symmetries due to ferroelectric distortions of tetragonal PbTiO$_3$ [see also Fig. 1]; therefore, ferroelectricity has only a slight influence on the thermodynamic stability of oxygen vacancies.

The Pb vacancies exhibit completely different energetics from the oxygen vacancies [see Fig. 3(c)]. The formation energies of V_{Pb}^0, V_{Pb}^-, and V_{Pb}^{2-} are almost the same and are high (6.1 eV) at the VBM, which indicates that it is difficult for Pb vacancies to form near the VBM. The formation energies of the charged Pb vacancies decrease as the Fermi level increases, which is opposite to dependence of the oxygen vacancy formation energy on the Fermi level. This is due to the opposite sign of the charge states of the vacancies (i.e., V_{Pb} is negatively charged, while V_{O1} and V_{O2} are positively charged). The formation energy of V_{Pb}^{2-} becomes negative near the CBM, which suggests that V_{Pb}^{2-} is stable and forms spontaneously during crystal growth near the CBM. However, V_{Pb}^- still possesses a high formation energy of 2.74 eV at the CBM, so that the singly ionized and neutral states are unlikely to be formed.

For the Ti vacancies, the formation energy exhibits similar behavior to that for Pb vacancies [see Fig. 3(d)]. However, the Ti vacancies have much higher formation energy than other vacancies in PbTiO$_3$. At the VBM, for example, the formation energy of a neutral Ti vacancy is lower than the other charge states, 11.2 eV. This is several times higher than that of other vacancies; therefore, the formation of Ti vacancies is much less possible near the VBM. In contrast, near the CBM, the relatively large charge state (maximally 4−) lowers

the formation energy of V_{Ti} significantly. In particular, the formation energy of V_{Ti}^{4-} is -0.89 eV at the CBM, which suggests that the formation of V_{Ti}^{4-} may be possible near the CBM.

Let us next compare the stability among all the vacancies in PbTiO$_3$. Figure 4 shows E_{vf} for V_{O1}, V_{O2}, V_{Pb}, and V_{Ti} as a function of ε_F under oxygen-poor (point A) and oxygen-rich (point D) conditions. At each Fermi level, we take the lowest formation energy among all the charge states for each vacancy. Under the oxygen-poor condition, the formation energies of V_{O1} and V_{O2} are negative over a wide range of Fermi levels ($\varepsilon_F < 1.8$ eV), whereas those for V_{Pb} and V_{Ti} are relatively large and positive. This indicates that oxygen vacancies can form spontaneously during crystal growth and become abundant, while the formation of V_{Pb} and V_{Ti} is strictly prohibited. V_{Pb} and V_{Ti} become stable and coexist only when the Fermi level is very close to the CBM ($\varepsilon_F > 3.0$ eV). Between these Fermi levels ($1.8 < \varepsilon_F < 3.0$ eV), all vacancies may have a small concentration, which makes it possible to grow fine PbTiO$_3$ crystals. In contrast, under the oxygen-rich condition, the stability range of V_{O1} and V_{O2} is significantly decreased and restricted to only the vicinity of the VBM ($\varepsilon_F < 0.5$ eV). Therefore, V_{O1} and V_{O2} become less stable than under the oxygen-poor condition. However, the formation energies of V_{Pb} and V_{Ti} become lower than those under the oxygen-poor condition, and their stability range is consequently expanded to $\varepsilon_F > 1.8$ eV. Thus, high-quality crystal growth is expected at lower Fermi levels of $0.5 < \varepsilon_F < 1.8$ eV.

These results are consistent with the relevant experimental observations; as the oxygen partial pressure increases (i.e., the condition changes from oxygen-poor to oxygen-rich), the concentration of oxygen vacancies decreases, but the number of metal vacancies increases.[4,5,7]

For the direct relevance with more realistic conditions, the defect-stability diagram (e.g., Brouwer diagram),[57] which describes defect stability as functions of temperature, oxygen partial pressure, and Fermi energy of the system, can be calculated by considering possible equilibrium chemical reactions pathways (laws of mass action)[58] under charge neutrality condition and evaluating the energetics of these chemical
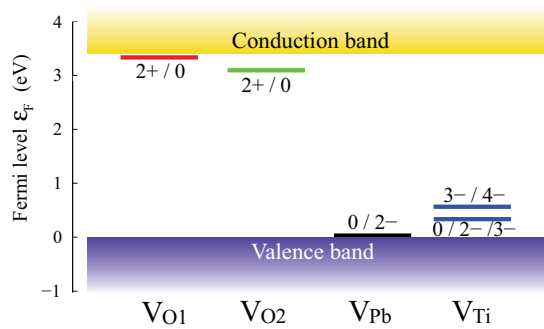
FIG. 5. (Color online) Defect transition levels of V_{O1}, V_{O2}, V_{Pb}, and V_{Ti} in ferroelectric $PbTiO_3$. Numbers on each transition level line indicate the change of charge state q.

reactions via first-principles calculations. Since the (partial) defect-stability diagram for oxygen defects in $SrTiO_3$ has been reported very recently,[59] the full defect-stability diagram for

all kinds of defects in $PbTiO_3$ will be addressed in a future work.

Another concern is about the way such defects can associate with each other (i.e., defect clustering). Some previous works addressed this issue in a similar way with the isolated vacancy in the present study but employed the simulation model, including two vacancies simultaneously.[60,61] In addition, the defect-clustering pathways can also be discussed by calculating energy barriers for possible defect-diffusion pathways.[62] This may be a possible future work to reveal the complicated defect physics in solids.

3. Charge states and transition levels

Here we discuss the possible charge states and transition levels of pre-existing or just-formed vacancies. Figure 5 depicts the defect-transition levels for each vacancy in ferroelectric $PbTiO_3$. The defect-transition level corresponds to the intersection of the vacancy formation energies for the different
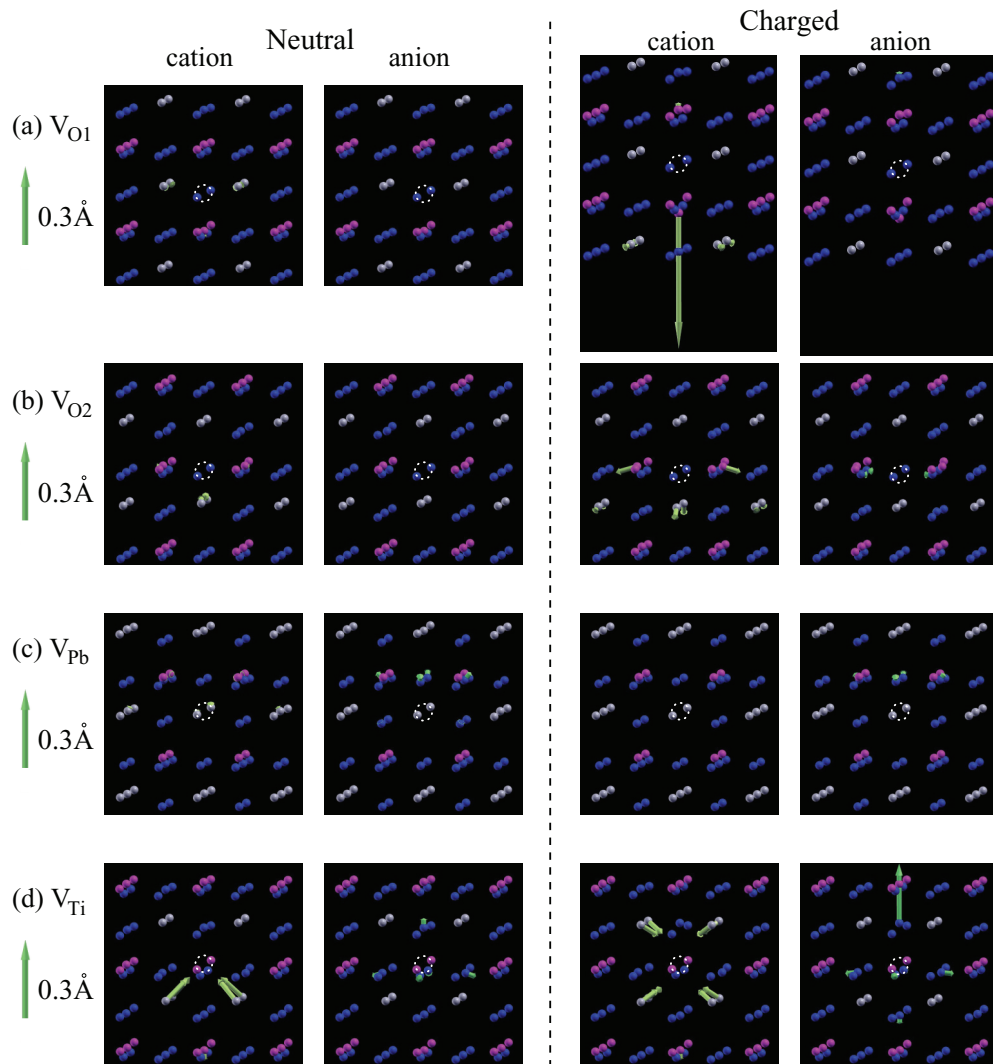
FIG. 6. (Color online) Cation and anion displacements around (a) V_{O1}, (b) V_{O2}, (c) V_{Pb}, and (d) V_{Ti} with respect to perfect (defect-free) ferroelectric $PbTiO_3$. Only the $2 \times 2 \times 2$ unit-cell-area centering each vacancy is shown for clarity. Dashed circles indicate the position of the vacancy site. For comparison, the spontaneous displacements of Ti, O1, and O2 with respect to Pb in perfect $PbTiO_3$ are 0.190 Å, 0.518 Å, and 0.532 Å, respectively.

TABLE III. Magnetic moment per vacancy, M, of V_{O1}, V_{O2}, V_{Pb}, and V_{Ti} in ferroelectric $PbTiO_3$.

Vacancy	V_{O1}^0	V_{O1}^+	V_{O1}^{2+}	V_{O2}^0	V_{O2}^+	V_{O2}^{2+}		
M (μ_B)	0.0	1.0	0.0	0.0	1.0	0.0		
Vacancy	V_{Pb}^0	V_{Pb}^-	V_{Pb}^{2-}	V_{Ti}^0	V_{Ti}^-	V_{Ti}^{2-}	V_{Ti}^{3-}	V_{Ti}^{4-}
M (μ_B)	0.0	1.0	0.0	4.0	3.0	2.0	1.0	0.0

charge states [see also Fig. 3]. V_{O1} has a $2+/0$ transition level at only 0.06 eV below the CBM, which indicates that V_{O1} behaves as a double-shallow donor that releases two electrons. Similarly, V_{O2} possesses a $2+/0$ transition level at a slightly deeper level of 0.3 eV below the CBM and thus also acts as a double shallow donor. This corresponds well to the experimentally observed n-type conductivity in a $PbTiO_3$ sample under lead-rich (oxygen-poor) conditions.[19,20] The double-shallow-donor nature is also reported for an oxygen vacancy in $BaTiO_3$.[29] However, for V_{Pb}, a $0/2-$ transition level is evident in the vicinity of the VBM, which indicates that V_{Pb} behaves as a double-shallow acceptor that traps two electrons and induces holes in $PbTiO_3$. Consequently, V_{Pb} can exhibit p-type (hole) conductivity. V_{Ti} has two distinct transition levels in the band gap: a $0/2-/3-$ transition at

0.45 eV above the VBM and a $3-/4-$ transition at 0.68 eV above the VBM. This implies that V_{Ti} may also exhibit acceptorlike behavior. However, the formation energy of V_{Ti} near the VBM is much higher than that of V_{Pb} [see also Fig. 4], which suggests that p-type conductivity in $PbTiO_3$ would predominantly result from the contributions of Pb vacancies rather than Ti vacancies. These results are consistent with the experimental observations of p-type conductivity in a $PbTiO_3$ sample with abundant Pb vacancies.[4,5]

B. Atomic structures of vacancies and ferroelectric disturbance

Figure 6 shows the displacement of cations (Pb and Ti) and anions (oxygen) around V_{O1}, V_{O2}, V_{Pb}, and V_{Ti} in ferroelectric $PbTiO_3$. Here, the atomic displacement from the perfect (defect-free) $PbTiO_3$ is visualized to extract the intrinsic effect of a vacancy, and only the $2 \times 2 \times 2$ unit cell area centering each vacancy is shown for clarity. Note that the effect of the vacancy ranges within two-unit-cell lengths at most. For V_{O1}^0, the cations are slightly displaced along almost $[00\bar{1}]$, and the displacement is highly confined to the vacancy site, while the oxygens do not move appreciably. Since ferroelectricity is due to the relative displacement of cations with respect to anions in crystals, the displacement
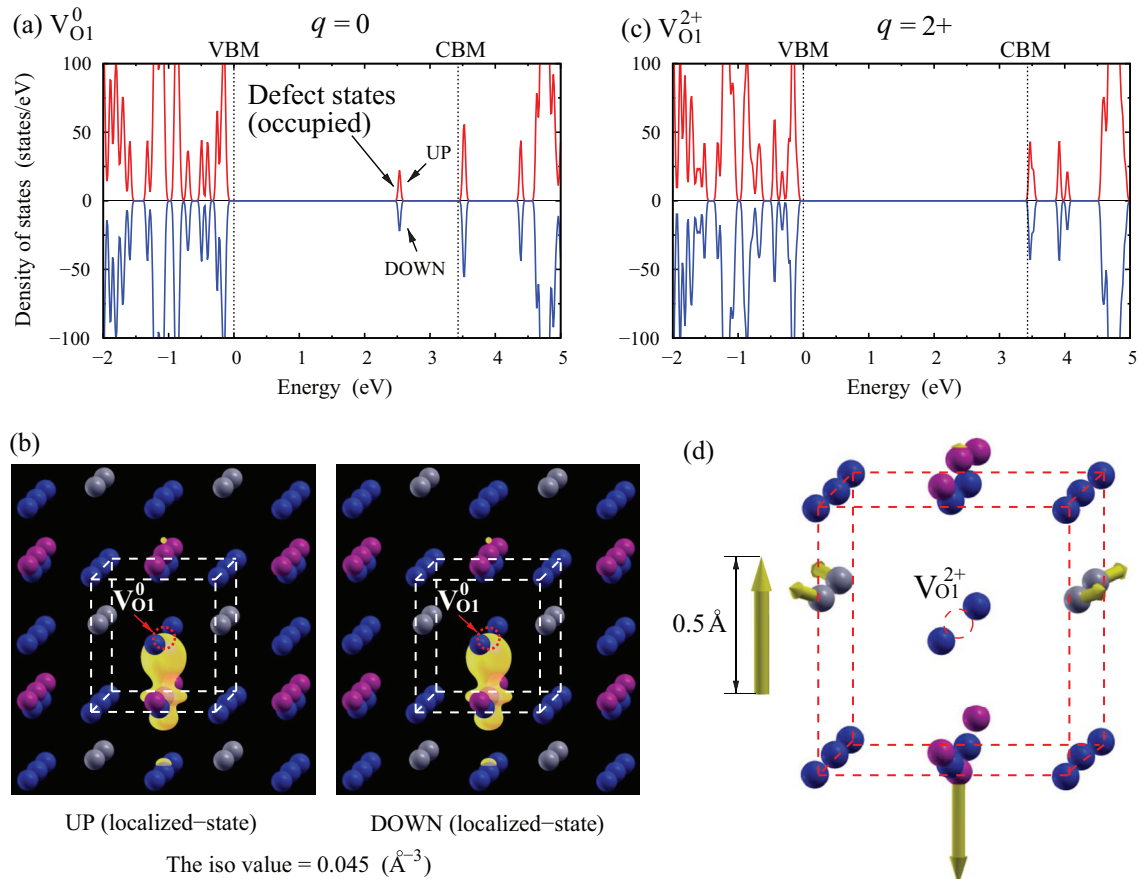
FIG. 7. (Color online) Electronic structures and atomic displacements of V_{O1} in ferroelectric $PbTiO_3$. (a) DOS of the neutral vacancy V_{O1}^0, (b) spatial distribution of the squared wave functions $|\psi_e|^2$ of the occupied defect states of V_{O1}^0 (yellow iso-surface), (c) DOS of the positively charged vacancy V_{O1}^{2+}, and (d) atomic displacement around V_{O1}^{2+} relative to V_{O1}^0.

of cations around V_{O1}^0 corresponds to the opposite direction to the spontaneous polarization along [001]. The presence of V_{O1}^0 thus suppresses ferroelectricity. This ferroelectric disturbance is significantly enhanced when the O1 vacancy is $2+$ charged. In particular, the displacement of Ti just below V_{O1}^0 (0.498 Å) is opposite to and larger than the spontaneous displacement of Ti in perfect PbTiO$_3$ (0.190 Å), which suggests that the polarization locally inverse to the intrinsic polar direction. This also implies that V_{O1}^{2+} may become a possible origin of polarization switching from [001] to [00$\bar{1}$]. In contrast, V_{O2} induces the ferroelectric disturbance perpendicular to the polar axis [see Fig. 6(b)]. The magnitude of this disturbance is enhanced when the O2 vacancy is positively charged, which is the same trend as that for the O1 vacancy. In contrast to the anisotropic and outward ferroelectric disturbance by the oxygen vacancies, an inward disturbance is evident around both V_{Pb} and V_{Ti}. However, the ferroelectric disturbance of V_{Pb} is still very small and almost unchanged when V_{Pb} is $2-$ charged, while the disturbance is enhanced with charged V_{Ti}^{4-}, which is in common with V_{O1} and V_{O2}. Thus, the ferroelectric disturbance is strongly dependent on the type of vacancy. Note that the local polarization concept,[63–69] which can evaluate the cell-by-cell polarization, cannot be applied to the deficient systems, such as in the present models, because the local polarization concept requires the unit cell-containing perfect (stoichiometric) PbTiO$_3$.

C. Magnetic moments induced by vacancies

Table III lists the magnetic moments of each vacancy in ferroelectric PbTiO$_3$. Although ferroelectric PbTiO$_3$ is intrinsically nonmagnetic, we found that some vacancies drive magnetization. For the neural oxygen vacancy that releases two electrons, the magnetic moment is zero, while the magnetic moment of 1.0 μ_B appears when the oxygen vacancy is singly charged. The oxygen vacancy turns to nonmagnetic when it is $2+$ charged. The similar trend is found for the Pb vacancy. On the other hand, the neutral Ti vacancy possesses the magnetic moment of 4.0 μ_B. The magnetic moment monotonically decreases as the Ti vacancy is charged negatively. These magnetic properties of vacancies are closely related to the defect electronic states discussed in the next section.

D. Electronic structures and defect states

Here, we first provide detailed defect electronic structures for each native vacancy in ferroelectric PbTiO$_3$. Figure 7 shows the electronic and atomic structures of V_{O1} in ferroelectric PbTiO$_3$. From the density of states (DOS) of the neutral V_{O1}^0, an electronic state can be determined between the VBM and CBM [Fig. 7(a)], which cannot be observed in perfect (defect-free) PbTiO$_3$. Therefore, this is a defect electronic state induced by V_{O1}^0. The defect state is located at 2.56 eV above the VBM and is occupied by two electrons. To obtain further details, the
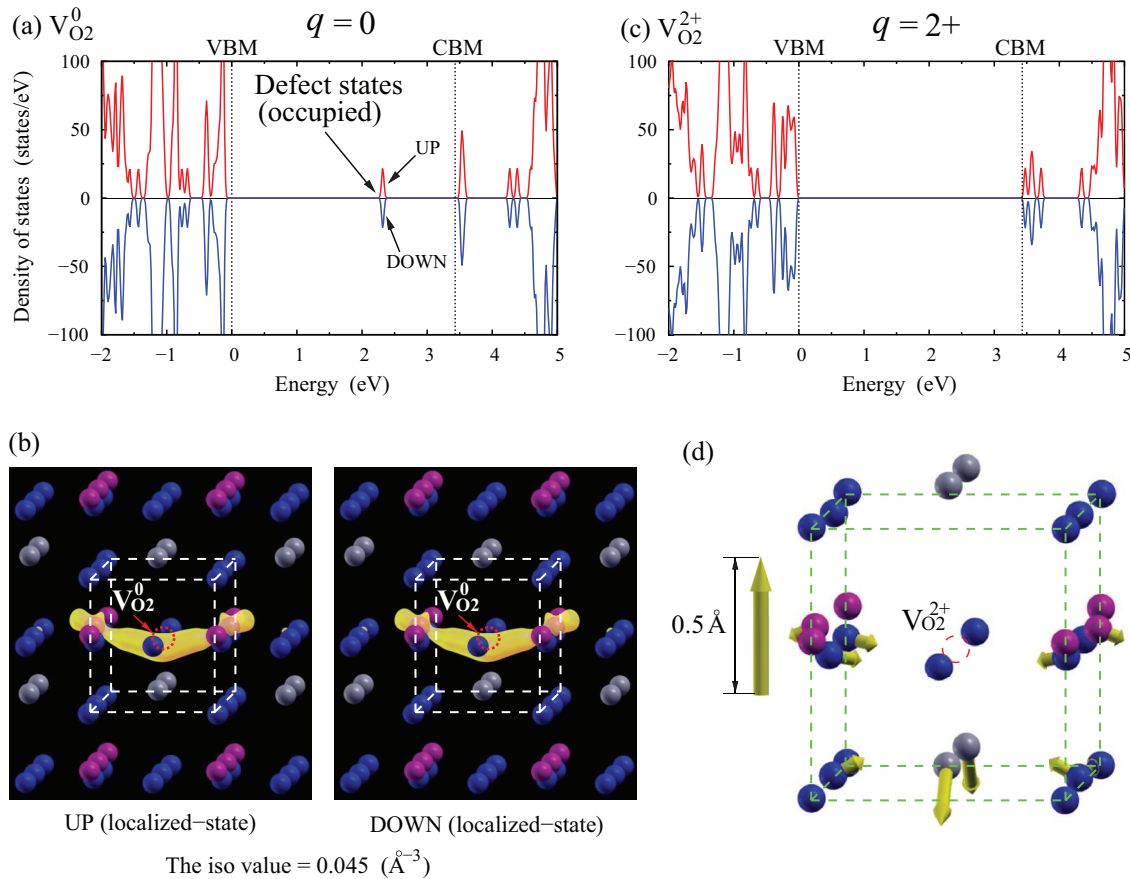
FIG. 8. (Color online) Electronic structures and atomic displacements of V_{O2} in ferroelectric PbTiO$_3$. (a) DOS of the neutral vacancy V_{O2}^0, (b) spatial distribution of the squared wave functions $|\psi_e|^2$ of the occupied defect states of V_{O2}^0 (yellow iso-surface), (c) DOS of the positively charged vacancy V_{O2}^{2+}, and (d) atomic displacement around V_{O2}^{2+} relative to V_{O2}^0.

squared wave function $|\psi_e|^2$ of the defect state is visualized in Fig. 7(b). The defect state is highly confined around V_{O1}^0 and the neighboring Ti atom in $[00\bar{1}]$, which suggests that V_{O1}^0 induces a localized defect state. It is also clearly evident from the shape of wave function that the d_{z^2} orbital is the main contributor to the defect state. Considering that the Ti d_{z^2} and O1 p_z orbitals are hybridized and form a $pd\sigma$ bond in perfect (defect-free) PbTiO$_3$,[15,16] a loss of the $pd\sigma$ bond due to the O1 vacancy may induce the d_{z^2}-contributed defect state at the Ti atom. This result is consistent with the experimental observation that Ti^{4+} is reduced to Ti^{3+} in oxygen-deficient octahedra by charge compensation.[70] In contrast, for charged V_{O1}^{2+}, no defect state is observed within the band gap [Fig. 7(c)], because when the O1 vacancy is $2+$ charged by releasing two electrons, the defect state becomes unoccupied and shifts its energy level to above the CBM. The absence of the localized defect state in V_{O1}^{2+} makes the O1 vacancy site positively charged, which leads to repulsive force between V_{O1}^{2+} and the cations (Ti and Pb) through Coulombic interaction. The Ti atom below the O1 vacancy, where the defect state is localized in the neutral state, is significantly displaced in the downward direction [Fig. 7(d)], as described in Sec. III B.

Figure 8 shows the electronic and atomic structures of V_{O2} in ferroelectric PbTiO$_3$. Similar to the case of V_{O1}^0, neutral V_{O2}^0 induces a defect state occupied by two electrons at 2.32 eV

above the VBM [Fig. 8(a)]. The defect state is highly localized between V_{O2}^0 and two neighboring Ti atoms and is contributed to by the $d_{x^2-y^2}$ orbital [Fig. 8(b)]. As the Ti $d_{x^2-y^2}$ orbital hybridizes with the O2 p_x orbital in defect-free PbTiO$_3$,[15,16] the defect state of V_{O2}^0 may also be induced by a loss of a hybridized p-d bond. When the O2 vacancy is $2+$ charged, the defect state is unoccupied, and the vacancy site is positively charged [Fig. 8(c)]. As a result, cationic Pb and Ti atoms, and anionic O atoms neighboring V_{O2}^{2+}, are displaced outward and inward, respectively. Note that the atomic displacement is almost along the [100] direction, which corresponds to the [100]-oriented distribution of the defect state [Figs. 8(b) and 8(d)]. Thus, the nature of the defect states explains why V_{O2} induces the ferroelectric disturbance perpendicular to the polar axis.

In contrast to the oxygen vacancies, the cation (Pb and Ti) vacancies exhibit distinct characteristics of defects states. V_{Pb}^0 forms an unoccupied defect state at 0.34 eV above the VBM [Fig. 9(a)]. Unlike the oxygen vacancies, where the defect states are highly localized at the vacancy site, the defect state is spatially distributed away from V_{Pb}^0 [Fig. 9(b)], i.e., the delocalized state. When the Pb vacancy is $2-$ charged by trapping two electrons, the defect state is fully occupied, and the energy level is shifted to below the VBM [Fig. 9(c)]. However, the atomic structure remains almost unchanged by
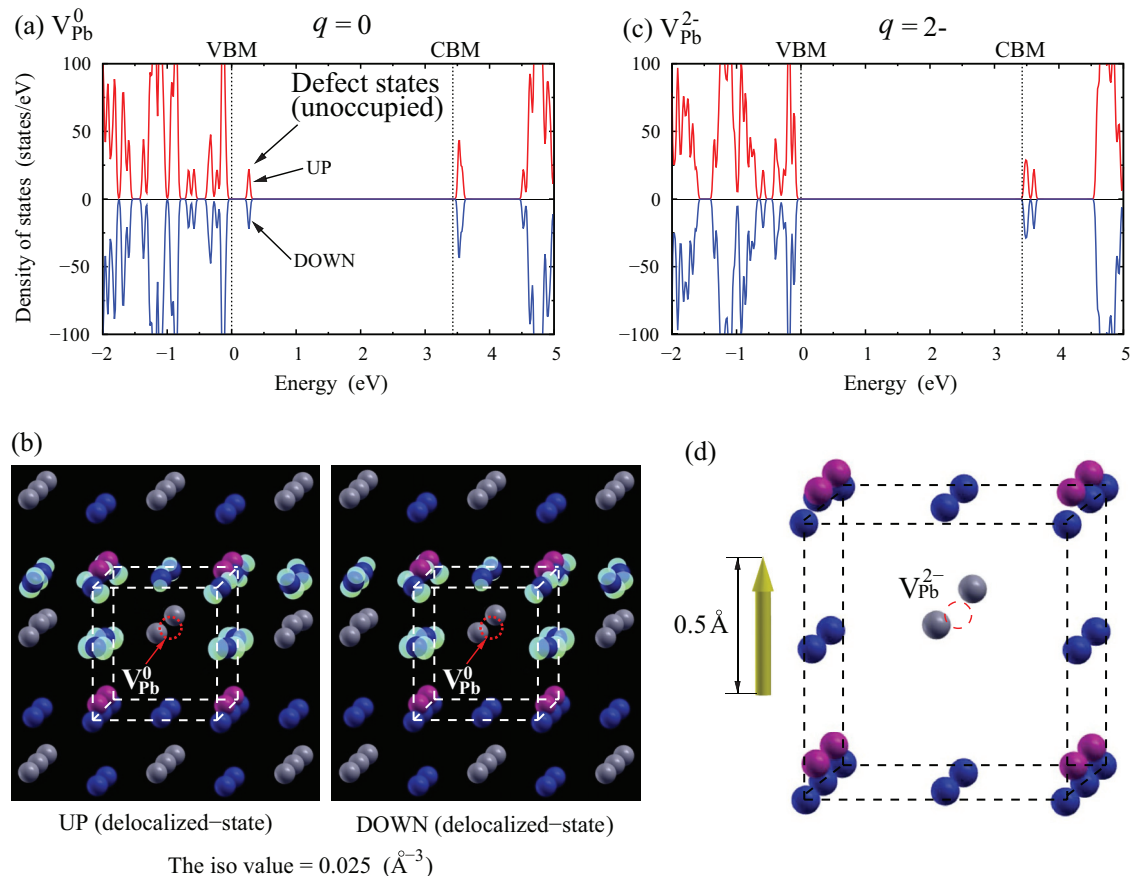
FIG. 9. (Color online) Electronic structures and atomic displacements of V_{Pb} in ferroelectric PbTiO$_3$. (a) DOS of the neutral vacancy V_{Pb}^0, (b) spatial distribution of the squared wave functions $|\psi_e|^2$ of the unoccupied defect states of V_{Pb}^0 (green iso-surface), (c) DOS of the negatively-charged vacancy V_{Pb}^{2-}, and (d) atomic displacement around V_{Pb}^{2-} relative to V_{Pb}^0.

the charging (the atomic displacement is smaller than that in oxygen vacancies by two orders of magnitude) [Fig. 9(d)]. This is because the electrons that occupy the defect states are not localized but distribute spatially away from the vacancy site [see also Fig. 9(b)].

Distinctively, V_{Ti}^0 induces four unoccupied defect states, in each of which two are degenerate [Fig. 10(a)]. The doubly degenerate defect states with a lower energy level (0.65 eV above the VBM), which are denoted as L1 and L2, exhibit a delocalized character [Fig. 10(b)]. On the other hand, the other doubly degenerated defect states with a relatively higher energy level (0.90 eV above the VBM), which are denoted

as H1 and H2, are highly localized at the O1 atom above the V_{Ti}^0 site. The defect states of H1 and H2 exhibit p_x and p_y orbital characteristics, respectively. The O1 p_x and p_y orbitals are hybridized with the Ti d_{zx} and d_{yz} orbitals, respectively; therefore, by forming a $pd\pi$ bond in defect-free PbTiO$_3$, these defect states are closely related to the loss of a bond due to V_{Ti}^0. The Ti vacancy is negatively charged, so that the defect states are occupied from the lower to higher levels and shift the energy levels down below the VBM [Fig. 10(c)]. By occupying these defect states, negative charges are concentrated, especially at the O1 atom above the V_{Ti}^{4-} site. The anionic Pb atoms are thus displaced inward
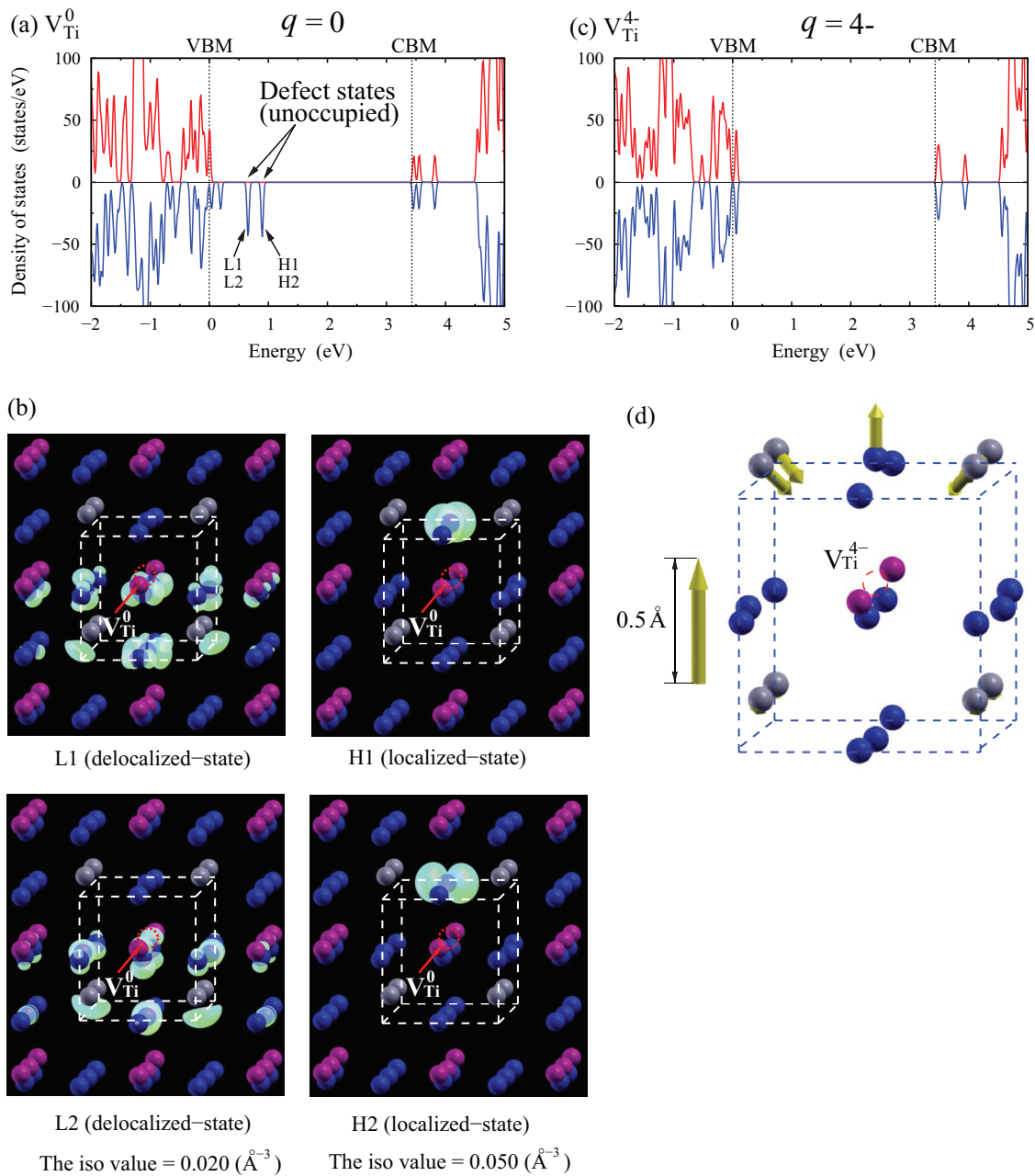
FIG. 10. (Color online) Electronic structures and atomic displacements of V_{Ti} in ferroelectric PbTiO$_3$. (a) DOS of the neutral vacancy V_{Ti}^0, (b) spatial distribution of the squared wave functions $|\psi_e|^2$ of the unoccupied defect states of V_{Ti}^0 (green iso-surface), (c) DOS of the negatively charged vacancy V_{Ti}^{4-}, and (d) atomic displacement around V_{Ti}^{4-} relative to V_{Ti}^0.

to the O1 atom, while the cationic oxygen moves outward [Fig. 10(d)].

Thus, the characteristics of the defect electronic states (localized/delocalized) are dependent on the type of vacancy, and the defect states are directly associated with the ferroelectric disturbance by a vacancy through its charge distribution. In addition, the defect states are closely related to the orbitals that contribute to a hybridized bond in perfect PbTiO$_3$. It should be noted the present hybrid-functional calculations indicate that the defect states are all induced in the band gap, which is common in oxide materials.[26–29] However, no clear defect state was obtained in the band gap using the LDA functional.[38] For oxygen vacancies, the DOS from the LDA functional seem to capture not the defect state itself, but the conduction-band edge, because the intrinsic defect state is embedded in the conduction bands due to underestimation of the band gap. Such an incorrect pictures of the defect electronic structure when employing the LDA or GGA functionals have also been reported for various oxide materials,[26–29] which suggests that the use of the hybrid functional, as in the present work, is essential for the study of defect physics.

IV. CONCLUSION

The energetic, ferroelectric, and electronic properties of intrinsic-point defects in ferroelectric PbTiO$_3$ with different charge states were investigated using first-principles calculations based on the HSE06 hybrid HF density functionals. The HSE06 hybrid functional accurately reproduces the band gap of PbTiO$_3$, which enables a correct description of the defect electronic states.

The oxygen vacancies are determined to act as double-shallow donors and are thermodynamically stable over a wide range of Fermi level under oxygen-poor conditions, while the Pb and Ti vacancies are likely to form under oxygen-rich conditions. The Pb vacancy acts as a double-shallow acceptor, which leads to *p*-type conductivity. The results correspond well with the relevant experimental observations.[4,5]

The ferroelectric distortion is anisotropically disturbed outward by oxygen vacancies, while an isotropically inward ferroelectric disturbance is evident around Pb and Ti vacancies. Such a ferroelectric disturbance is strongly enhanced by the charging of vacancies, except for the Pb vacancy, where no significant change is observed.

The oxygen vacancies induce the defect electronic state in the middle of the band gap, which is strongly localized at the neighboring Ti atom and is contributed to by the *d* orbital. The localized defect state may result from a partial loss of the Ti-O bond through the hybridization of Ti-*d* and O-*p* orbitals due to oxygen vacancy formation. In contrast, the defect state of the Pb vacancy exhibits a delocalized character. The Ti vacancy induces localized and delocalized defect states, both of which are doubly degenerate. These distinct defect-state characteristics explain why the ferroelectric disturbance is completely different and dependent on the type of vacancy.

*Corresponding author: shimada@me.kyoto-u.ac.jp

[1] M. E. Lines and A. M. Glass, *Principles and Applications of Ferroelectrics and Related Materials* (Clarendon, Oxford, 1979).

[2] R. Ramesh, *Thin Film Ferroelectric Materials and Devices* (Kluwer Academic, Boston, 1997).

[3] J. F. Scott, *Ferroelectric Memories* (Springer, Berlin, 2000).

[4] R. Gerson, J. Appl. Phys. **31**, 188 (1960).

[5] R. Gerson and H. Jaffe, J. Phys. Chem. Solids **24**, 979 (1963).

[6] S. K. Hau and K. H. Wong, Appl. Phys. Lett. **66**, 245 (1995).

[7] A. K. Tagantsev, I. Stolichnov, and N. Setter, J. Appl. Phys. **90**, 1387 (2001).

[8] W. L. Warren, D. Dimos, and R. M. Waser, MRS Bull. **21**, 40 (1996).

[9] J. F. Scott and M. Dawber, Appl. Phys. Lett. **76**, 3801 (2000).

[10] W. L. Warren, H. N. Al Shareef, D. Dimos, B. A. Tuttle, and G. E. Pike, Appl. Phys. Lett. **68**, 1681 (1996).

[11] S. Pöykkö and D. J. Chadi, Phys. Rev. Lett. **83**, 1231 (1999).

[12] L. He and D. Vanderbilt, Phys. Rev. B **68**, 134103 (2003).

[13] X. Du and I. Wei Chen, J. Appl. Phys. **83**, 7789 (1998).

[14] G. Burns and B. A. Scott, Phys. Rev. Lett. **25**, 1191 (1970).

[15] R. E. Cohen, Nature (London) **358**, 136 (1992).

[16] Y. Kuroiwa, S. Aoyagi, A. Sawada, J. Harada, E. Nishibori, M. Takata, and M. Sakata, Phys. Rev. Lett. **87**, 217601 (2001).

[17] R. Resta, M. Posternak, and A. Baldereschi, Phys. Rev. Lett. **70**, 1010 (1993).

[18] W. Zhong, R. D. King-Smith, and D. Vanderbilt, Phys. Rev. Lett. **72**, 3618 (1994).

[19] V. P. Afanasjev, I. P. Pronin, and A. L. Kholkin, Phys. Solid State **48**, 1214 (2006).

[20] V. P. Afanasjev, A. A. Petrov, I. P. Pronin, E. A. Tarakanov, E. J. Kaptelov, and J. Graul, J. Phys.: Condens. Matter **13**, 8755 (2001).

[21] P. Hohenberg and W. Kohn, Phys. Rev. **136**, B864 (1964).

[22] W. Kohn and L. Sham, Phys. Rev. **140**, A1133 (1995).

[23] D. M. Ceperley and B. J. Alder, Phys. Rev. Lett. **45**, 566 (1980).

[24] J. P. Perdew, J. A. Chevary, S. H. Vosko, K. A. Jackson, M. R. Pederson, D. J. Singh, and C. Fiolhais, Phys. Rev. B **46**, 6671 (1992).

[25] J. P. Perdew, K. Burke, and M. Ernzerhof, Phys. Rev. Lett. **77**, 3865 (1996).

[26] A. Janotti, J. B. Varley, P. Rinke, N. Umezawa, G. Kresse, and C. G. Van de Walle, Phys. Rev. B **81**, 085212 (2010).

[27] F. Oba, A. Togo, I. Tanaka, J. Paier, and G. Kresse, Phys. Rev. B **77**, 245202 (2008).

[28] P. Agoston, K. Albe, R. M. Nieminen, and M. J. Puska, Phys. Rev. Lett. **103**, 245501 (2009).

[29] M. Choi, F. Oba, and I. Tanaka, Appl. Phys. Lett. **98**, 172901 (2011).

[30] T. Shimada, X. Wang, S. Tomoda, P. Marton, C. Elsässer, and T. Kitamura, Phys. Rev. B **83**, 094121 (2011).

[31] C. H. Park and D. J. Chadi, Phys. Rev. B **57**, R13961 (1998).

[32] S. Pöykko and D. J. Chadi, Appl. Phys. Lett. **76**, 499 (2000).

[33] Z. Zhang, P. Wu, L. Lu, and C. Shu, Appl. Phys. Lett. **88**, 142902 (2006).

[34] P. Erhart, R.-A. Eichel, P. Träskelin, and K. Albe, Phys. Rev. B **76**, 174116 (2007).

[35] Z. Alahmed and H. Fu, Phys. Rev. B **76**, 224101 (2007).

[36] Z. Zhang, P. Wu, L. Lu, and C. Shu, J. Alloys Compd. **449**, 362 (2008).

[37] Y. Yao and H. Fu, Phys. Rev. B **84**, 064112 (2011).

[38] T. Shimada, Y. Uratani, and T. Kitamura, Appl. Phys. Lett. **100**, 162901 (2012).

[39] T. Shimada, Y. Uratani, and T. Kitamura, Acta Materialia **60**, 6322 (2012).

[40] J. Robertson, W. L. Warren, and B. A. Tuttle, J. Appl. Phys. **77**, 3975 (1995).

[41] J. Heyd, G. E. Scuseria, and M. Ernzerhof, J. Chem. Phys. **118**, 8207 (2003); **124**, 219906 (2006).

[42] J. Paier, M. Marsman, K. Hummer, G. Kresse, I. C. Gerber, and J. G. Ángyán, J. Chem. Phys. **124**, 154709 (2006); **125**, 249901 (2006).

[43] G. Kresse and J. Hafner, Phys. Rev. B **47**, 558 (1993).

[44] G. Kresse and J. Furthmüller, Phys. Rev. B **54**, 11169 (1996).

[45] P. E. Blöchl, Phys. Rev. B **50**, 17953 (1994).

[46] G. Kresse and D. Joubert, Phys. Rev. B **59**, 1758 (1999).

[47] S. A. Mabud and A. M. Glazer, J. Appl. Crystallogr. **12**, 49 (1979).

[48] J. P. Perdew, A. Ruzsinszky, G. I. Csonka, O. A. Vydrov, G. E. Scuseria, L. A. Constantin, X. Zhou, and K. Burke, Phys. Rev. Lett. **100**, 136406 (2008).

[49] S. L. Dudarev, G. A. Botton, S. Y. Savrasov, C. J. Humphreys, and A. P. Sutton, Phys. Rev. B **57**, 1505 (1998).

[50] E. Pavarini, S. Biermann, A. Poteryaev, A. I. Lichtenstein, A. Georges, and O. K. Andersen, Phys. Rev. Lett. **92**, 176403 (2004).

[51] H. J. Monkhorst and J. D. Pack, Phys. Rev. B **13**, 5188 (1976).

[52] J. Lento, J.-L. Mozos, and R. M. Nieminen, J. Phys.: Condens. Matter **14**, 2637 (2002).

[53] G. Makov and M. C. Payne, Phys. Rev. B **51**, 4014 (1995).

[54] P. Erhart, K. Albe, and A. Klein, Phys. Rev. B **73**, 205203 (2006).

[55] M. Choi, F. Oba, and I. Tanaka, Phys. Rev. B **78**, 014115 (2008).

[56] W. M. Haynes, *CRC Handbook of Chemistry and Physics*, 92nd ed. (CRC Press, Boca Raton, 2007).

[57] G. Brouwer, Philips Res. Rep. **9**, 366 (1954).

[58] M. W. Barsoum, *Fundamentals of Ceramics* (Institute of Physics Publishing, New York, 1997).

[59] A. Samanta, W. E, and S. B. Zhang, Phys. Rev. B **86**, 195107 (2012).

[60] D. D. Cuong, B. Lee, K. M. Choi, H.-S. Ahn, S. Han, and J. Lee, Phys. Rev. Lett. **98**, 115503 (2007).

[61] P. Erhart and K. Albe, J. Appl. Phys. **102**, 084111 (2007).

[62] A. V. Kimmel, P. M. Weaver, M. G. Cain, and P. V. Sushko, Phys. Rev. Lett. **109**, 117601 (2012).

[63] T. Shimada, Y. Umeno, and T. Kitamura, Phys. Rev. B **77**, 094105 (2008).

[64] T. Shimada, S. Tomoda, and T. Kitamura, Phys. Rev. B **81**, 144116 (2010).

[65] B. Meyer and D. Vanderbilt, Phys. Rev. B **65**, 104111 (2002).

[66] T. Shimada, S. Tomoda, and T. Kitamura, J. Phys.: Condens. Matter **22**, 355901 (2010).

[67] T. Shimada, X. Wang, Y. Kondo, and T. Kitamura, Phys. Rev. Lett. **108**, 067601 (2012).

[68] G. Pilania and R. Ramprasad, Phys. Rev. B **82**, 155442 (2010).

[69] T. Shimada, S. Tomoda, and T. Kitamura, Phys. Rev. B **79**, 024102 (2009).

[70] D. I. Woodward, I. M. Reaney, G. Y. Yang, E. C. Dickey, and C. A. Randall, Appl. Phys. Lett. **84**, 4650 (2004).